Flexible Resistive Sensor Developed with Printed Electronics Technologies

Invited Paper

Damian Ricalde
Dto. Prototipado Microelectrónico y Electrónica Impresa
Instituto Nacional de Tecnología Industrial
Buenos Aires, Argentina
dricalde@inti.gob.ar

Julián Marinoni
Dto. Prototipado Microelectrónico y Electrónica Impresa
Instituto Nacional de Tecnología Industrial
Buenos Aires, Argentina
marinoni@inti.gob.ar

Mariano Roberti
Dto. Prototipado Microelectrónico y Electrónica Impresa
Instituto Nacional de Tecnología Industrial
Buenos Aires, Argentina
froberti@inti.gob.ar

Fabrizio Pascual
Horacio Berardi
Ingeniería Electrónica
Universidad Nacional de San Martín (UNSAM)
Buenos Aires, Argentina
fberardi@estudiantes.unsam.edu.ar

Theo Rodríguez Campos
Dto. Prototipado Microelectrónico y Electrónica Impresa
Instituto Nacional de Tecnología Industrial
Buenos Aires, Argentina
trodriguez@inti.gob.ar

Alex Lozano
DT. de Micro y Nanotecnologías
Instituto Nacional de Tecnología Industrial
Buenos Aires, Argentina
alozano@inti.gob.ar

Liliana Fraigi
Escuela de Ciencia y Tecnología UNSAM
Dto de Electrónica
Universidad Nacional Tecnológica – UTN-FRBA
Buenos Aires, Argentina
lili@frba.utn.edu.ar

Mijal Mass
Dto. Prototipado Microelectrónico y Electrónica Impresa
Instituto Nacional de Tecnología Industrial
Buenos Aires, Argentina
*mmass@inti.gob.ar

2025 Argentine Conference on Electronics (CAE) | 979-8-3315-2263-6/25/$31.00 ©2025 IEEE | DOI: 10.1109/CAE64243.2025.10961962

***Abstract*— Flexible resistive sensors have a wide range of applications, from monitoring human joint movements to measuring industrial mechanical parameters. This paper describes the analysis, design, fabrication, and characterization of a low-cost, lightweight resistive sensor, screen-printed on a flexible substrate. The proposed design enables the adjustment of final resistance value by modifying only one mask in the manufacturing process. A high-precision flexible sensor was obtained, with less than 0.3% of spread, capable of detecting at least four different curvature radii (125, 90, 65, and 50mm), in addition to the resting state (r∞), and enduring over a thousand flexion cycles while maintaining its performance. These sensors were developed at the Printed Electronics Pilot Plant of the National Institute of Industrial Technology (INTI).**

Keywords*— printed electronics, flexible sensor, resistive sensor, functional printing, additive manufacturing.

I. Introduction

The constant advancement of technology and the increasing automation in the industrial sector present both opportunities and challenges in the development of flexible electronic devices. In particular, flexible sensors have gained prominence in various applications due to their flexibility, elasticity, and stability. Their relevance is crucial in human motion detection [1,2], clinical monitoring and diagnostics [3, 4], the development of adaptable electronic skin (e-skin) [5], the implementation of flexible touchscreens [6], and even integration into industrial robots [7].

Among the different types of flexible sensors, resistive sensors stand out for their ability to measure changes in electrical resistance in response to mechanical deformations. This property makes them ideal for applications requiring high sensitivity and precision, making them essential components in monitoring and control systems [8]. Additionally, Printed Electronics (PE) emerges as an innovative technology capable of meeting the requirements of these resistive sensors, offering advantages such as low manufacturing costs, large-area processability, reduced carbon footprint, and high physical flexibility.

In this work, we present the analysis, design, fabrication, and characterization of flexible printed resistive sensors (FPRS) for use in measuring joint movements through rehabilitation gloves, robotic arms, exoskeletons, and gesture-controlled interaction/interface devices.

II. Experimental

A. Design

To evaluate the change in resistance of the flexible printed resistive sensors (FPRS) as a function of deformation, a sensor was designed with 14 series-connected resistors measuring 5mm × 5mm (Lc × W), linked by conductors of 1mm (L_{Ag}) × 5mm (W). This configuration results in a sensor with an active area length of 84mm and a total length of 91mm, including the contact pads, as shown in "Fig. 1". This design allows for adjusting the total resistance value by modifying only the L_{Ag} length of the conductive layer, Metal 2 ("Fig. 2c").

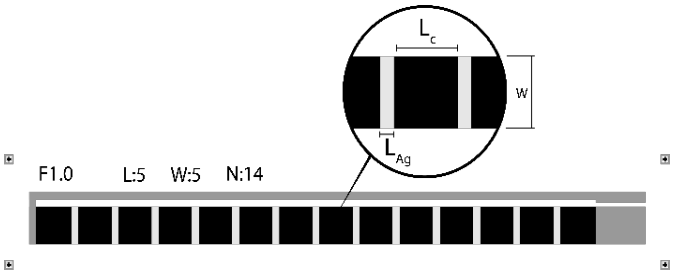

Fig. 1. Design of the flexible printed resistive sensor (FPRS) with detailed dimensions of L_{Ag}, L_c y W.

"Fig. 2" illustrates the three layers that compose the sensor. "Fig. 2a" shows the mask design for the first conductive layer (Metal 1), "Fig. 2b" depicts the resistive layer, and "Fig. 2c" presents the final conductive layer (Metal 2), which is printed over the resistive layer. This manufacturing sequence enables the production of a family of FPRS with the same length but different final resistance values by modifying only L_{Ag}.

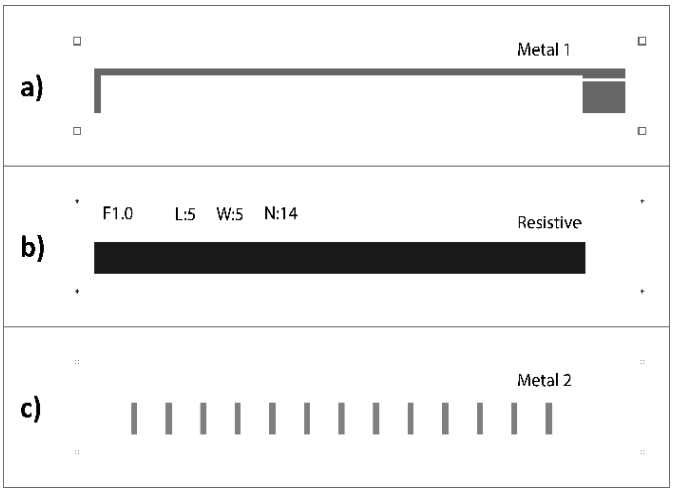

Fig. 2. Mask design of the flexible printed resistive sensor: (a) Metal 1; (b) Resistive layer; (c) Metal 2.

The different sensor layers were designed using a free and open-source vector graphics editor (Inkscape). The masks were fabricated by a national printing company on a film with a resolution of 3600 dpi.

B. Materials and printing process

Screen printing was selected as the manufacturing process for the FPRS. A semi-automatic screen printer (EKRA Microtronic II) was used, adjusting printing parameters (pressure, speed, snap-off distance, squeegee material) to achieve the dimensional accuracy and characteristic thickness of the process.

For sensor fabrication, a silver-based conductive ink (SCAG-003, Mateprincs) and a carbon-based resistive ink (C2030519P4, Gwent) were used. Based on the specifications from their datasheets, meshes with the appropriate thread count per inch were selected for each ink. The design transfer onto these meshes was carried out through a photolithographic process using a 50 µm photosensitive film (*Ulano*®).

Printing was performed on 100 µm thick polyethylene terephthalate (PET) substrates. Ink curing was carried out in a Thermical TH400DH drying oven, with modified curing conditions—extending the curing time and reducing the temperature—to avoid altering the substrate properties (TABLE I).

TABLE I . CURING TIMES AND TEMPERATURES FOR THE INKS USED IN SENSOR FABRICATION

Ink	Curing
Conductor (Silver) (Mateprincs-SCAG-003)	60' @ 80°C
Resistive (Carbon) (Gwent-C2030519P4)	30' @ 60°C

Finally, the FPRS were laminated using 3M 467MP double-sided adhesive with a QDTM Flexo flexographic tester, applying a pressure of 1.26 kgf/cm² onto a 250µm thick PET (Mylar® cristal, Decom) to enhance the sensor's rigidity and stability. The final length of the manufactured FPRS device is 110mm..

III. CHARACTERIZATION

Once the sensors were fabricated, both dimensional and electrical characterization was performed.

A. Dimensional Characterization

The dimensions of the mask designs and their transfer onto the meshes and prints were measured and compared along the X and Y axes using the fiducial camera of a Dimatix DMP-2850 inkjet printer, with micrometric resolution. For thickness characterization, an interferometry profilometer (Zeiss model 5104802) was used.

B. Electrical characterization

A Keithley 2602B Source Measure Unit (SMU) was used in a 2-wire configuration, as the sensor resistance exceeded 1kΩ.

Electrical characterization by mechanical strain is essential to understand how these sensors respond to controlled deformation forces or dynamic mechanical characterization. For that purpose, an automated system was developed using a Nema 17 stepper motor and parallel flat-face clamps. This system enabled cyclic testing of the FPRS, ensuring precise (6.78µm per step) and repeatable testing conditions. Additionally, it eliminated the need to manually handle the samples for each connection and disconnection ("Fig. 3").

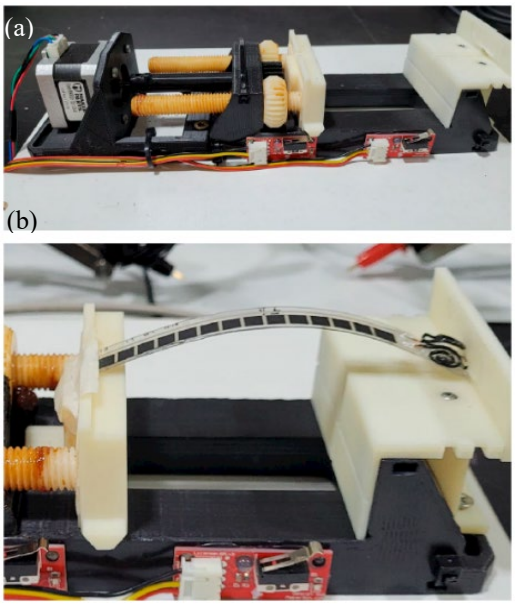

Fig. 3. Automated characterization system. (a) Mechanical testing bench (b) Dynamic characterization of a flexible printed resistive sensor fabricated via screen printing using Ag and C inks.

Using this dynamic characterization system, we measured the key comparison parameter, that is the curvature radius the sensor assumes when bent. This parameter is mathematically related to the bending angle through the arc length of a circumference (“Fig. 4”) and can be calculated using equation (1).

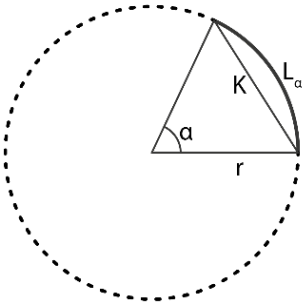

Fig. 4. Chord diagram of a circumference, where r represents the curvature radius, Lα is the arc length, α is the angle, and K is the chord length connecting two points on the circumference without passing through the center.

$$\alpha = \frac{L_\alpha}{r} \quad (1)$$

Since the characterization system generates an axial movement, the control variable, K, was derived using trigonometric relationships, as shown in equation (2).

$$K = 2 \cdot r \cdot \sin\frac{\alpha}{2} \quad (2)$$

Based on preliminary characterizations, where no significant resistance variations were observed for curvature radii greater than 150mm, the starting radius for testing was set at 125mm.

Finally, four curvature radii were established: 125mm (r125), 90mm (r90), 65mm (r65), and 50mm (r50), in addition to the resting state (r_∞). Measurements were performed as shown in “Fig. 5”. It should be noted that, between consecutive measurements, the sensor remained at rest for 5 seconds, while a 90-second rest period was maintained between test cycles.

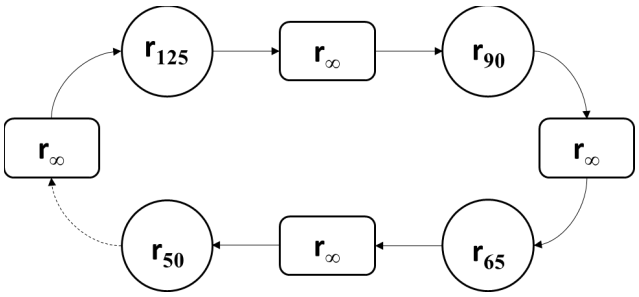

Fig. 5. Diagram of a complete measurement cycle. 300 cycles were repeated for each FPRS.

Three FPRS with the same design and fabrication process were tested, with each cycle being repeated 300 times to determine the resistance variation for each measurement point.

C. Gauge Factor

To determine the sensitivity of these sensors, the Gauge Factor was calculated using the "beam theory" as a deformation model (“Fig. 6”).

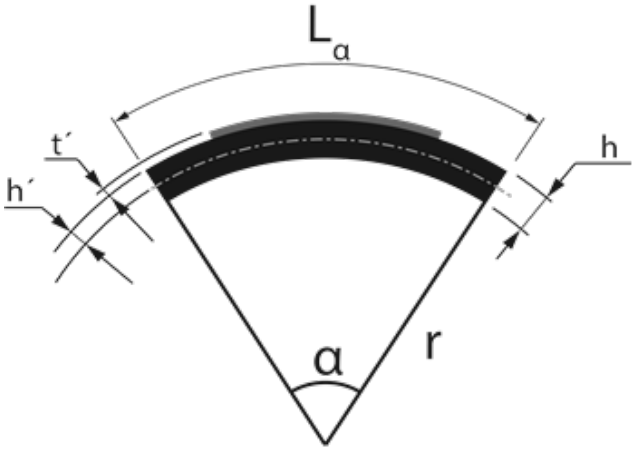

Fig. 6. Deformation model, where r is the curvature radius under flexion, h is the substrate thickness, h' is the distance from a point on the neutral axis to the surface where the printed film is deposited, t' is the thickness of the printed film, and Lα is the sensor length.

The sensors were subjected to a force perpendicular to their longitudinal axis, causing compression in the lower fibers and elongation in the upper fibers, where the sensitive printed film

is located. This interaction between compression and tension is referred to as bending stress (“Fig. 7”)

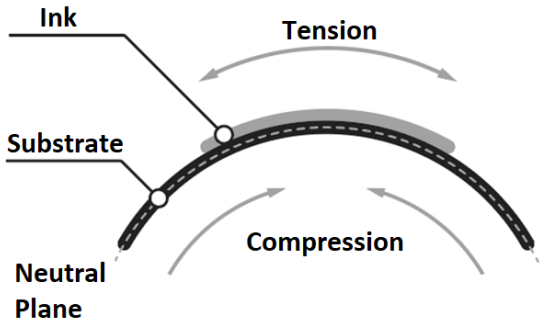

Fig. 7. Schematic of a flexible printed sensor exposed to bending stress.

Considering the Navier-Bernoulli hypothesis and some additional considerations, the deformation was estimated using equations (3) and (4):

$$\varepsilon = -\frac{h'}{r} \quad compression \tag{3}$$

$$\varepsilon = \frac{h'}{r} \quad tension \tag{4}$$

where h' represents the distance from the neutral axis to the surface where the printed film is deposited, and r is the curvature radius of the centroidal axis of the prism.

Assuming that the sensitive layer thickness is negligible compared to the sensor substrate ($t' \ll h$) and that $r \gg h/2$, equation (4) was rewritten to describe the maximum deformation experienced by the outermost surface using equation (5):

$$\varepsilon = \frac{h'}{r} = \frac{h/2}{r} \tag{5}$$

Then, the Gauge Factor (GF) is defined as the ratio between the relative change in electrical resistance ($\Delta R/R$) and the mechanical strain ($\boldsymbol{\varepsilon}$) according to equation (6).

$$FG = \frac{\Delta R/R}{\varepsilon} \tag{6}$$

Substituting (5) into (6) results in equation (7), which enables the calculation of the FPRS sensitivity via the Gauge Factor.

$$FG = \frac{\Delta R/R \cdot (2r)}{h} \tag{7}$$

Finally, the stability of sensor resistance under no deformation was analyzed as a function of temperature variations. Samples were exposed to temperatures ranging from 25°C to 65°C in 5°C increments, allowing stabilization at each measurement point before recording the values.

IV. Results

The dimensional and electrical characterization yielded the following results.

A. Dimensional Characterization

A reduction of approximately 30 µm was observed in the sensor dimensions along the X and Y axes. This variation represents a change of less than 1%, which is considered negligible for the functionality of these devices. Moreover, this value falls within the error margins of the technology used.

The thickness measurement results are presented in TABLE II:

TABLE II – Ink thickness in printed sensors.

Ink	Average thickness [µm]
Conductor (Silver) (Mateprincs-SCAG-003)	29
Resistive (Carbon) (Gwent-C2030519P4)	27

B. Electrical Characterization

“Fig. 8” shows the average, maximum, and minimum resistance variations of the sensors as a function of the established curvature radii.

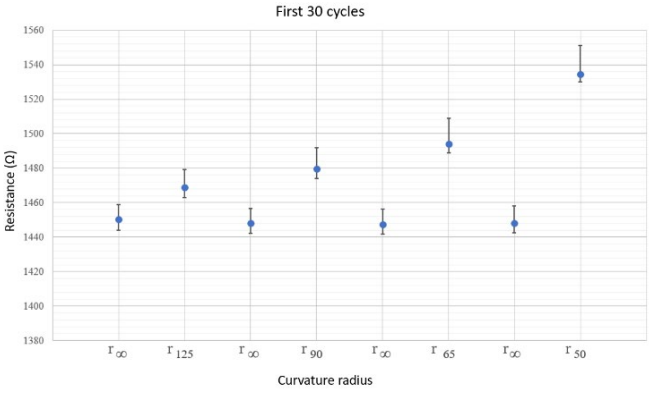

Fig. 8. Graph of resistance values obtained during the first 30 cycles.

During the first 30 cycles, the average resistance values for each curvature radius (blue markers) indicate a variation in the resistance of the FPRS. However, due to the high measurement dispersion, the obtained values are very close to the minimum values of the next higher curvature radius. This high dispersion maintains a clear differentiation of the sensor’s deformation level.

After 300 cycles for each sensor, a significant reduction in measurement dispersion was observed for each curvature radius, resulting in five well-differentiated points, as shown in "Fig. 9".

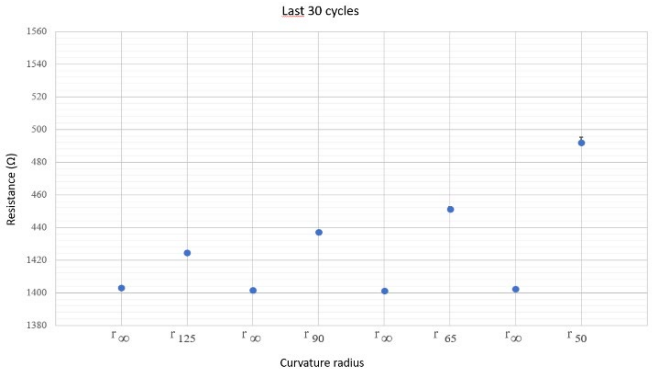

Fig. 9. Graph of resistance values obtained during the last 30 cycles.

Comparing the initial measurements with the final ones (Fig. 8 and 9), it was observed that the resistance values and their dispersions tend to decrease, reaching dispersion values in the range of 0.28% to 0.06%.

C. Gauge Factor

The strain was calculated using equation (5), and the Gauge Factor was determined using equation (7) as a function of different curvature radii. The results are presented in Table III.

TABLE III – STRAIN AND GAUGE FACTOR RESULTS FOR FPRS.

Bending radius [mm]	Deformation [με]	Gauge Factor		
		FPRS I	*FPRS II*	*FPRS III*
125	1595	12.3	13.7	14.2
90	2212	12.3	14.2	15.0
65	3058	12.0	14.2	15.2
50	3968	15.4	18.9	19.4

These results indicate that for the first three curvature radii, the obtained GF values are similar, and this trend was consistent across all three sensors.

This behavior suggests that from the resting state up to a curvature radius of 65mm, the sensors exhibit a proportional elastic response, which means they follow Hooke's Law. However, between 65mm and 50mm, the sensors maintain their elastic behavior (as they always return to the same resting resistance value) but no longer exhibit a linear response. In both cases, the sensor material remains within an reversible elastic regime.

Plotting ΔR/R as a function of strain, for example, in FPRS I, considering the four curvature radii (125, 90, 65, and 50mm), the best-fit linear trendline achieves an R^2 value of approximately 0.95. However, when excluding the 50mm curvature radius, the linear trend line fit improves to an R^2 value above 0.99 ("Fig. 10").

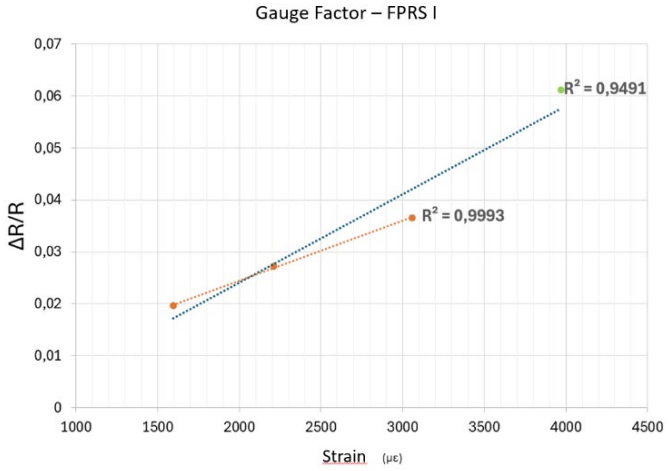

Fig. 10. Comparison of linearity considering curvature radii of 125, 90, 65 and 50mm (blue trend line) and only the first three (125, 90 and 65mm) (orange trend line).

Regarding thermal characterization, the resistance values did not exhibit any significant changes with increasing temperature.

V. CONCLUSIONS

As a result of this work, the following conclusions can be drawn:

- A series of flexible printed resistive sensors (FPRS) was successfully developed using a low-cost screen-printing process, making it feasible for local and regional production.

- A versatile design was achieved, allowing easy modification of the final resistance value by adjusting only one mask in the device's manufacturing process.

- A set of flexible printed resistive sensors was fabricated and characterized, demonstrating the ability to accurately distinguish resistance variations for curvature radii of 125mm, 90mm, 65mm, and 50mm, as well as in their resting position (r_∞).

- The sensors improved in precision as the number of flexion cycles increased, achieving a dispersion of less than 0.3% after 300 cycles.

- The fabricated sensors endured more than 1,000 flexion cycles without performance degradation, indicating a long operational lifespan.

- The obtained sensors exhibited a Gauge Factor (GF) between 12 and 15, achieving a sensitivity seven times higher than traditional metal strain gauges.

- Thermal characterization results showed that the sensor resistance remained stable within the tested temperature range (25°C to 65°C), with no significant variations.

ACKNOWLEDGMENT

The authors would like to thank the students of the Electronic Technology courses, cohort 2023, of the Electronic Engineering program at UTN-FRBA for their collaboration.

REFERENCES

[1] C. Huang, G. Yang, P. Huang, J. Hu, Z. Tang, Y. Li, and S. Fu, “Flexible Pressure Sensor with an Excellent Linear Response in a Broad Detection Range for Human Motion Monitoring,” *ACS Applied Materials & Interfaces*, vol. 15, no.2, Jan., 2023.

[2] L. Duan, D. R. D'hooge, and L. Cardon, “Recent progress on flexible and stretchable piezoresistive strain sensors: From design to application,” *Progress in Materials Science*, vol. 114, Oct., 2023.

[3] J. Yan, A. Chen, and S. Liu, “Flexible sensing platform based on polymer materials for health and exercise monitoring,” *Alexandria Engineering Journal*, vol. 86, Sep., pp. 405-414, 2023.

[4] N. Wen, L. Zhang, D. Jiang, Z. Wu, B. Li, C. Sun, and Z. Guo, “Emerging flexible sensors based on nanomaterials: recent status and applications,” *Journal of Materials Chemistry A*, vol. 8, Nov., pp. 25499-25527, 2020.

[5] P. Nie, R. Wang, X. Xu, Y. Cheng, X. Wang, L. Shi, and J. Sun, “High-Performance Piezoresistive Electronic Skin with Bionic Hierarchical Microstructure and Microcracks, ” *ACS Applied Materials & Interfaces*, vol. 9, no. 17, Apr., 2017.

[6] C. Ouyang, D. Liu, K. He, and J. Kang, "Recent Advances in Touch Sensors for Flexible Displays," *IEEE Open Journal of Nanotechnology*, vol. 4, pp. 36-46; 2022.

[7] J. Min, J. Pack, H. I. Park, and Y. Cha, “Classification of Floor Materials Using Piezoelectric Actuator–Sensor Pair and Deep Learning for Mobile Robots, ” *IEEE Access*, vol. 12, pp. 28511-28519, 2024.

[8] Z. Feng, Z. Liu, T. Shao, and Y. Zhang, “Application of nanomaterials in flexible sensors,” *Application of nanomaterials in flexible sensors*, vol. 23, pp. 162-169, 2023.

.